

This is a repository copy of *Threshold and power of pulsed red-emitting diode lasers with a bulk active layer near p-cladding under high-temperature operation.*

White Rose Research Online URL for this paper:

<https://eprints.whiterose.ac.uk/201712/>

Version: Published Version

Article:

Ryvkin, B. S. and Avrutin, Evgeny orcid.org/0000-0001-5488-3222 (2023) Threshold and power of pulsed red-emitting diode lasers with a bulk active layer near p-cladding under high-temperature operation. *Optical and quantum electronics*. 640. pp. 639-640. ISSN 0306-8919

<https://doi.org/10.1007/s11082-023-04887-6>

Reuse

This article is distributed under the terms of the Creative Commons Attribution (CC BY) licence. This licence allows you to distribute, remix, tweak, and build upon the work, even commercially, as long as you credit the authors for the original work. More information and the full terms of the licence here:

<https://creativecommons.org/licenses/>

Takedown

If you consider content in White Rose Research Online to be in breach of UK law, please notify us by emailing eprints@whiterose.ac.uk including the URL of the record and the reason for the withdrawal request.



Threshold and power of pulsed red-emitting diode lasers with a bulk active layer near *p*-cladding under high-temperature operation

Boris S. Ryvkin¹ · Eugene A. Avrutin²

Received: 6 March 2023 / Accepted: 25 April 2023 / Published online: 23 May 2023
© The Author(s) 2023

Abstract

Threshold properties and pulsed output of AlGaInP visible-emitting lasers with an asymmetric waveguide structure and a bulk active layer are analysed. The effects of the current leakage, increased by the heating of the laser due to the proximity of the electrical pulse source and the Joule heating in and around this source are analysed. When optimising the laser design, waveguiding properties of the bulk active layer are shown to be important, leading to threshold currents decreasing, and injection efficiency increasing, with active layer thickness in lasers with moderately thick ($< 0.1 \mu\text{m}$) active layers.

Keywords Semiconductor lasers · AlGaInP · Double heterostructure · Electron leakage · Internal efficiency

1 Introduction

In the previous papers (see Ryvkin et al. 2020; Avrutin et al. 2021; Avrutin and Ryvkin 2022) and references therein), we proposed and analysed a high-power semiconductor laser design using an asymmetric large optical cavity waveguide (with different refractive index steps at the interfaces between the Optical Confinement Layer (OCL) and the *n*- and *p*-claddings, and a relatively thick (typically bulk) active layer (AL) positioned very near the *p*-cladding. The design was shown to offer a number of advantages for lasers operating in a pulsed regime at wavelengths from visible (red) (Avrutin and Ryvkin 2022) through near infrared (800–900 nm (Avrutin et al. 2021)) to the eye safe wavelengths ($\sim 1.5 \mu\text{m}$ (Ryvkin et al. 2020), as confirmed by the recent experimental results (Hallman et al. 2019, 2021)). Specifically for red lasers, an important advantage of this design, in addition to single transverse mode operation with a relatively narrow far field, included a suppressed current leakage and hence improved injection efficiency at high pulse power. No threshold current densities and, correspondingly, output powers were calculated in Avrutin and

✉ Eugene A. Avrutin
eugene.avrutin@york.ac.uk

¹ A F Ioffe Physico-Technical Institute, St. Petersburg, Russia

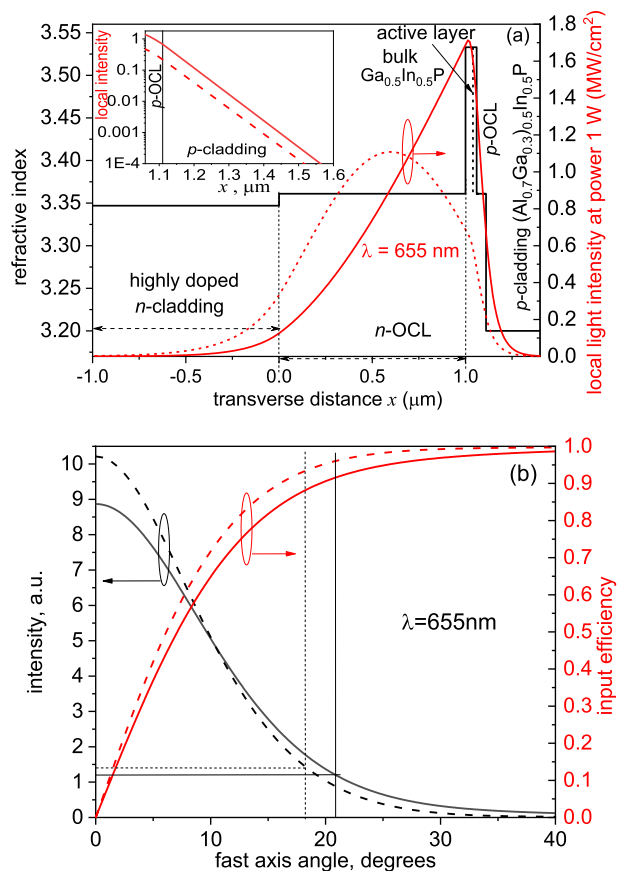
² School of Physics, Engineering, and Technology, University of York, York, UK

Ryvkin (2022); besides, temperature dependence of laser performance was not investigated in detail. The possible applications of red lasers (which include sensing including time of flight metrology, as well as photodynamic therapy (Miyamoto et al. 1999; Algorri et al. 2021; Hagimoto et al. 2023)) may however require operation at elevated temperatures, either ambient or current-induced, so low temperature sensitivity is highly desirable and merits further investigation which is the subject of this paper. Here, we present the analysis of the threshold current and light–current characteristics of lasers of this design under different pulsed operated conditions, including those leading to laser heating, study the effect of this heating on the optimal laser design, and show that this design promises competitive performance at elevated power operation.

2 Laser structure

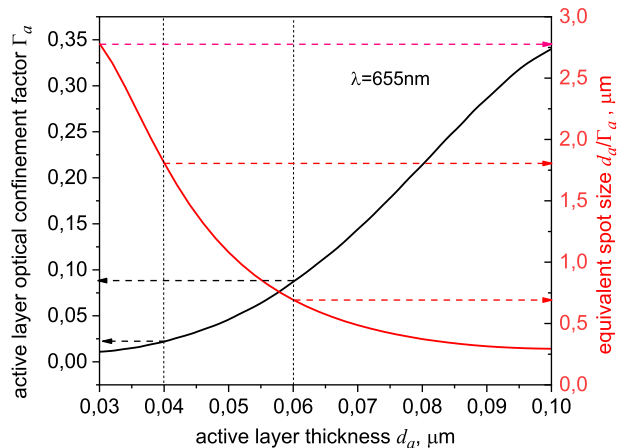
The refractive index profile of the structure considered is essentially the same as used in Avrutin and Ryvkin (2022) and is reproduced schematically in Fig. 1a for convenience, alongside the near field (transverse mode intensity profile) of the laser emission, with the inset magnifying the field in the *p*-cladding. The corresponding far field properties are

Fig. 1 **a** The waveguide structure of the proposed laser and the profile of modal intensity for the active layer thickness $d_a=0.06\ \mu\text{m}$ (solid) and $0.04\ \mu\text{m}$ (dashed), with the inset highlighting mode penetration into the *p*-cladding. **b** The corresponding vertical (fast axis) far field profiles and estimated input efficiency. Thin lines indicate the width of the far field at $1/e^2$ level



illustrated in Fig. 1b. Figure 1 represents a visible-emitting Ga_{0.5}In_{0.5}P/(Al_xGa_{1-x})_{0.5}In_{0.5}P (lattice matched to GaAs) laser with a bulk AL, with the same composition as that used in some earlier papers (see e.g. (Ishikawa et al. 1991)), with a fully disordered (random) structure so designed to emit at λ≈650–660 nm at room temperature depending on the threshold carrier density value (Bour 1993). As in Avrutin and Ryvkin (2022), the waveguide used is a large optical cavity (LOC) strongly asymmetric one, with the refractive index step at the interface between the OCL and the *n*-cladding substantially smaller than that at the OCL/*p*-cladding interface. The bulk (GaInP) AL is positioned at a very short distance (≈50 nm) from the *p*-cladding (note that the location of the active layer, bulk or Quantum Well, near the *p*-cladding is currently widely accepted for high-power semiconductor lasers (Hallman et al. 2019, 2021; Crump et al. 2013; Yamagata et al. 2015; Hasler et al. 2014; Kaul et al. 2019)). As noted previously (Ryvkin et al. 2020; Avrutin et al. 2021; Avrutin and Ryvkin 2022), in a waveguide of this type, unlike in most structures with Quantum Well based active layers, the AL itself contributes noticeably to the waveguiding properties of the structure, strongly affecting the shape of the mode. Thus, the thickness *d_a* of the active layer becomes an important and useful parameter in varying and potentially optimising the laser design and properties. This is clearly seen in Fig. 1a, which shows transverse mode profiles at the same wavelength for two relatively close AL thickness values (*d_a*=600 Å=0.06 μm and *d_a*=400 Å=0.04 μm). The mode profiles for the two cases are substantially different, with the broader AL localising the mode much more pronouncedly within the OCL. This results in the superlinear dependence of the confinement factor *Γ_a* on the AL thickness *d_a*, discussed in Avrutin and Ryvkin (2022). This dependence for the proposed design is shown in Fig. 2 below alongside that of the equivalent spot size *d_d*/*Γ_a*, which is important when analysing the phenomenon of catastrophic optical damage in a laser structure. We note that, despite the substantially different near fields, the *far* fields for both values of *d_a* are still moderate (Fig. 1b), with the broader AL broadening the far field (measured at the level of *e*⁻²) only by a few degrees (from ≈37 for *d_a*=400 Å to ≈42 for *d_a*=600 Å). Integrating the far field gives the light collection efficiency estimate at the level of *e*⁻² of 0.94 and 0.92 respectively, close to the well-known figure of 0.95 for a Gaussian beam. The inset to Fig. 1a also illustrates the fact that for the range of *d_a* values of interest, the degree of penetration of the field into the *p*-cladding remains quite low and its decay quite fast – this means that the modal field reaching the lossy GaAs substrate

Fig. 2 Active layer optical confinement factor *Γ_a* and the equivalent spot size *d_d*/*Γ_a* as functions of the active layer thickness in the structure of Fig. 1

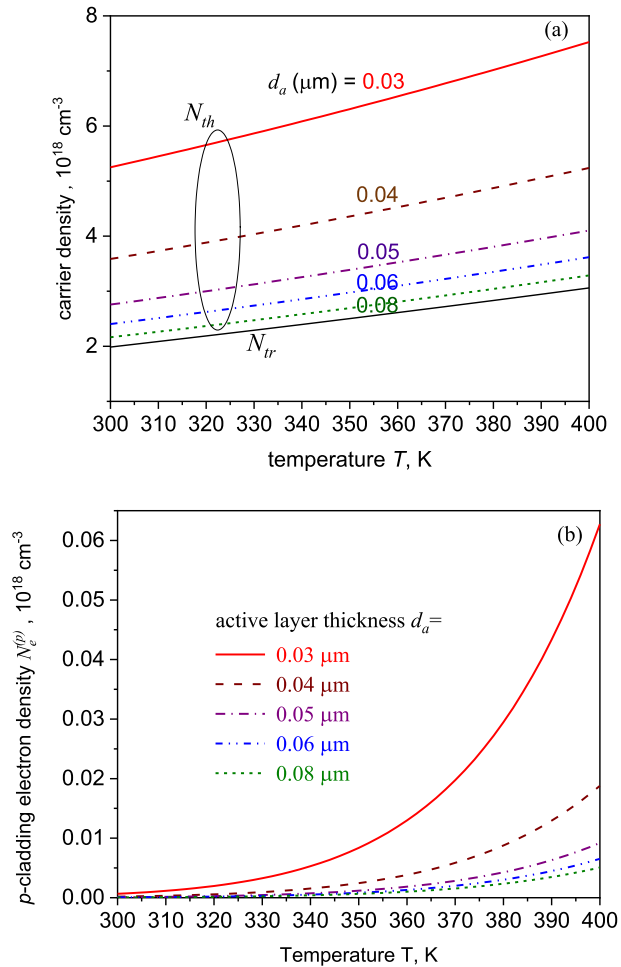


(Smowton et al. 2002) can be avoided while keeping the p -cladding quite thin, making for good electrical and thermal resistance.

3 Laser performance modeling.

The model for the properties of the active layer is similar to that used in Avrutin and Ryvkin (2022). The gain-carrier dependence is calculated within the usual microscopic model with a sech lineshape function. Given the bulk nature of the active layer, this dependence is approximated quite accurately by a linear expression $g(N) = \sigma_g(N - N_{tr})$, where, as in all materials, the gain cross-section σ_g decreases, and the transparency carrier density N_{tr} increases, with temperature. The two effects are known to add and thus to lead to an increase in the threshold carrier density

Fig. 3 **a** Transparency and threshold carrier density dependences on the temperature in the structure of Fig. 1, with a cavity loss of $\alpha = 9 \text{ cm}^{-1}$; **b**. Electron density at the p -cladding (near the interface with the p -OCL) as function of temperature in the same laser



$$N_{th} = N_{tr} + \frac{\alpha}{\Gamma_a \sigma_g} \tag{1}$$

(α being the total cavity loss) with temperature, as illustrated in Fig. 3a, which also shows the temperature dependence of N_{tr} . The dependences $N_{tr}(T)$ and $N_{th}(T)$ are both somewhat superlinear and, as can be expected, the temperature increase in N_{th} is the most pronounced for small values of d_a and hence of Γ_a . From $N_{th}(T)$ and T , as in Avrutin and Ryvkin (2022), we can determine the electron and hole quasi Fermi level separation $\Delta E_F^{(a)}$ in the AL which in turn defines the minority carrier (electron) density at the edge of the p -cladding (Agrawal and Dutta 1993; Smowton et al. 2002; Avrutin and Ryvkin 2022):

$$N_e^{(p)} = N_c^{(p)} \exp\left(-\frac{\delta E_{Fe}^{(p)}}{k_B T}\right) \tag{2}$$

Here, as in Avrutin and Ryvkin (2022), $N_c^{(p)}$ is the effective density of states of electrons in the p -cladding material, $\delta E_{Fe}^{(p)} = E_c^{(p)} - E_{Fe}$, > 0 is the difference between the energy $E_c^{(p)}$ of the lowest subband of the conduction band of the p -cladding material and the absolute position of the electron quasi Fermi level E_{Fe} . The value of $\delta E_{Fe}^{(p)}$ is determined by $\Delta E_F^{(a)}$ and the parameters (composition and doping) of the p -cladding, as discussed in Agrawal and Dutta (1993); Smowton et al. (2002); Avrutin and Ryvkin (2022).

The temperature dependence of $N_e^{(p)}$ is shown in Fig. 3b; note that it increases in temperature much more pronouncedly than either the transparency or threshold carrier density (as can be expected given the exponential function in Eq. (2)), meaning that the electron leakage current, which scales with $N_e^{(p)}$, is a rather strong function of temperature. This, in turn, leads to a strong decrease with temperature of the injection efficiency

$$\eta_i \approx \frac{1}{1 + \Delta} \tag{3}$$

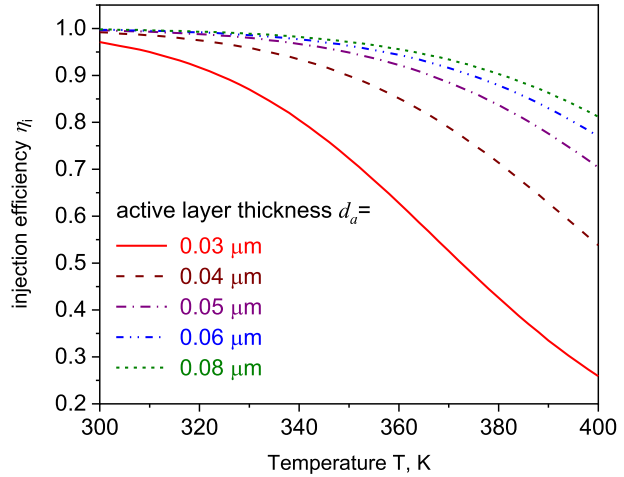
where

$$\Delta = \frac{\mu_e^{(p)} N_e^{(p)}}{\mu_h^{(p)} N_A^{(p)}} \tag{4}$$

is the ratio of the electron leakage current (the minority electron current in the p -cladding) to the majority hole current in the same cladding (Bour et al. 1993; Avrutin and Ryvkin 2022), $\mu_{e,h}^{(p)}$ being the corresponding mobility values. The temperature dependence of η_i is shown in Fig. 4 with d_a as a parameter. While a decrease in η_i with temperature is seen at all values of d_a , the effect is strongest for thin active layers ($d_a=0.03\text{--}0.04 \mu\text{m}$); for thicker active layers, the efficiency and depends much weaker on both temperature and d_a and remains reasonably high in the entire temperature range.

With the injection efficiency and the threshold carrier density known, we can evaluate the threshold current. Assuming good material quality (negligible Shockley-Reed-Hall recombination), and noting that Auger recombination is not significant in the broad-band-gap materials studied, the current density j_{th} and hence the total current i_{th} are evaluated from just the spontaneous recombination rate:

Fig. 4 Calculated injection efficiency as function of temperature in the structure of Fig. 1 at different values of the active layer thickness d_a

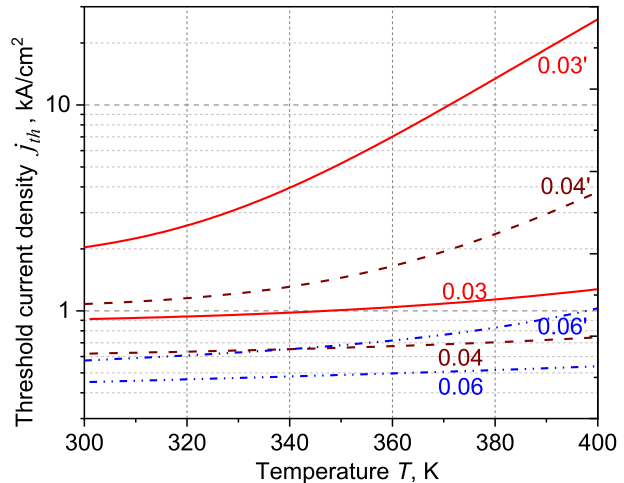


$$i_{th} = j_{th}wL; j_{th} \approx \frac{ed_a}{\eta_i(T)} \frac{B(T)N_{th}^2(T)}{1 + B_1(T)N_{th}(T)} \tag{5}$$

Here, L and w are the length of the laser resonator and the stripe width, respectively. The quadratic recombination coefficient B for the case of low carrier densities in a bulk material is known to scale with temperature as $B(T) \propto T^{-3/2}$ (we assumed the textbook value of $B = 1 \times 10^{10} \text{ cm}^3/\text{s}$ at $T = 300 \text{ K}$). The correction coefficient B_1 heuristically takes into account degenerate electron statistics and Coulomb interaction screening at high carrier densities (see e.g. (Olshansky et al. 1984) note the slightly different notations used in the current paper). Its temperature dependence is believed to be less pronounced than that of B ; we took a constant $B_1 = 10^{-19} \text{ cm}^3$ (Olshansky et al. 1984)).

The temperature dependences of the threshold current density for different values of d_a and for two cavity lengths (1 mm and 2 mm) are shown in Fig. 5. Somewhat

Fig. 5 Threshold current density as function of temperature in the structure of Fig. 1. Active layer thickness $d_a = 0.03 \mu\text{m}$ (solid), $0.04 \mu\text{m}$ (dashed), $0.06 \mu\text{m}$ (dash-dotted). Curve markings with a prime indicate the cavity length of 1 mm; without the prime, 2 mm



counterintuitively, despite the presence of d_a in the numerator of (5), for a given cavity length the threshold is noticeably lower for moderately thick active layers ($d_a=0.04\text{-}0.06\ \mu\text{m}$) than for thin ones ($d_a=0.03\ \mu\text{m}$); this is a direct result of the waveguide properties of the active layer (the increase of Γ_a with d_a). The increase in j_{th} with temperature is also less pronounced for larger d_a . We did not analyse the performance of active layers with d_a below $0.03\ \mu\text{m}$ as these would be essentially Quantum Wells and our bulk model would become tenuous, but as the tendencies discussed above appears quite robust, there is no reason to expect any qualitative changes.

Also seen in the figure is the fact that not only are the absolute values of threshold current lower for the larger values of d_a but their dependence on temperature also tends, overall, to be weaker.

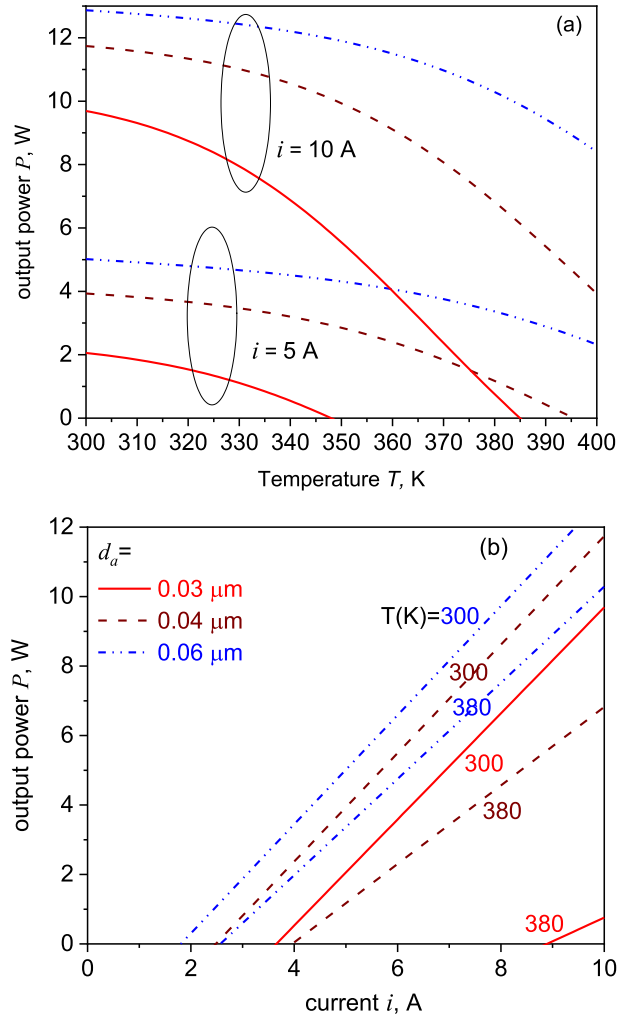
To compare the predicted temperature behaviour of threshold in the proposed design with that of existing Quantum Well lasers operating at similar wavelengths, we evaluated the characteristic temperature $T_0(T) = \left(\frac{d}{dT} \ln(j_{th}(T))\right)^{-1}$. Comparing the values of T_0 simulated for the proposed design with those reported for 1 mm long QW lasers operating at 650 nm (Dumitrescu et al. 1999), we note that the predicted T_0 values for our design at the high end (worst case) of the temperature range studied in Dumitrescu et al. (1999) (ambient temperature $T_a=60^\circ\text{C}$), for the same cavity length (1 mm), are $T_0=142\text{ K}$ ($d_a=0.04\ \mu\text{m}$) or $T_0=276\text{ K}$ ($d_a=0.06\ \mu\text{m}$) compared to $T_0=105\text{ K}$ measured in Dumitrescu et al. (1999) For 2 mm long lasers, our simulations at $T_a=60^\circ\text{C}$ give the values of $T_0=241\text{ K}$ for $d_a=0.04\ \mu\text{m}$ and $T_0=271\text{ K}$ for $d_a=0.06\ \mu\text{m}$. In QW lasers, operating at a similar wavelength ($\lambda=660\text{ nm}$), the value of $T_0=129\text{ K}$ has been measured at this temperature (Hagimoto et al. 2020). At higher still temperatures, $T_a=90^\circ\text{C}$ our predicted values fall to $T_0=113\text{ K}$ for $d_a=0.04\ \mu\text{m}$ and $T_0=181\text{ K}$ for $d_a=0.06\ \mu\text{m}$, but at least the latter remains substantially higher than $T_0=112\text{ K}$ measured for QW lasers (Hagimoto et al. 2020)).

As is well known, the temperature increase decreases the output power of a laser diode

$$P(i, T) = \frac{\hbar\omega}{e} \eta_{out} \eta_i(T) (i - i_{th}(T)) \tag{6}$$

Here, as usual, $\hbar\omega$ is the photon energy, $\eta_{out} = \alpha_{out}/\alpha = \alpha_{out}/(\alpha_{out} + \alpha_{in})$ is the output efficiency which, in this design, is to a good accuracy current-independent since the internal loss α_{in} is virtually entirely due to built-in losses (as opposed to carrier density dependent absorption as in longer-wavelength structures (Ryvkin et al. Aug 2020).) We assume the facet reflectance coefficients of $R_{AR}=0.05$, $R_{HR}=0.95$ which, for the length $L=2\text{ mm}$, gives the output loss $\alpha_{out}=7.6\text{ cm}^{-1}$; the internal loss was taken as $\alpha_{in}\approx 1.5\text{ cm}^{-1}$. In applications such as time of flight sensing/measurements (e.g. LIDAR), ambient temperatures of around -45°C to $+85^\circ\text{C}$ can be encountered, with the high end of this range being the dangerous one. Figure 6a demonstrates that for very thin AL, such heating can lead to a drastic decrease in the output power, up to and including complete laser shutdown, whereas the $d_a=0.06\ \mu\text{m}$ design promises much better temperature stability (Fig. 6a). If the temperature is treated as a fixed parameter so that $i_{th}(T) \neq f(i)$, the output characteristic for a given T is a straight line with the temperature dependence of the slope determined by $\eta_i(T)$ (Fig. 4) and the cutoff by $i_{th}(T)$ (Fig. 5). A family of such lines for different temperatures is presented in Fig. 6b for a range of elevated temperatures relevant for the applications. Under operating regimes where the heating is in part current-induced so $T=T(i)$ (e.g. either true CW operation or high repetition rate pulsed emission with the electric pulse source in close proximity to the laser), the dependences $P(i)$ at a given ambient temperature will become saturating or even nonmonotonic—but the qualitative tendencies with variation of

Fig. 6 Output power vs. temperature with current as parameter **a** and vs. current with temperature as parameter **b**. Active layer thickness $d_a=0.03\ \mu\text{m}$ (solid), $0.04\ \mu\text{m}$ (dashed), $0.06\ \mu\text{m}$ (dash-dotted). Cavity length $L=2\ \text{mm}$



d_a , according to preliminary simulations, do not change: the designs with the larger value of d_a can be expected to offer superior performance *at all operating conditions*.

Unfortunately, in practice it may not always be possible to utilise the advantage of the large d_a , because AlGaInP lasers considered here are well known to suffer significantly from Catastrophic Optical Degradation (COD) (see for example (BouSanayeh et al. 2006; Lichtenstein et al. 2000) and references therein). This is caused by extreme localised heating of material near the facets, which is determined by the internal power density (light intensity) *within the active layer* at the facet and presents a significant threat even under quasi-CW operation. Due to the localisation of the optical mode at the active layer, the COD danger can be expected to be more pronounced with $d_a=0.06\ \mu\text{m}$ than with the smaller two values shown. While it is difficult to analyse this effect qualitatively without experimental data on the exact material and structure parameters used here, some rough numerical estimates can be inferred from the experiments on different laser designs (Bou-Sanayeh et al. 2006; Lichtenstein et al. 2000; Sanchez et al. 2021). The results imply that

at least for the case of a wide ($w=200\ \mu\text{m}$) stripe presented in Fig. 6 and for relatively short pulse (a few ns) operation, the danger of COD for $d_a=0.03\text{--}0.04\ \mu\text{m}$ is not significant, but taking full advantage of $d_a=0.06\ \mu\text{m}$ may need some form of COD prevention (e.g. facet passivation).

In summary, we have analysed the threshold and efficiency of AlGaInP visible-emitting lasers with an asymmetric waveguide structure and a bulk active layer as functions of temperature, and calculated the output curves of the laser under pulsed operation and elevated temperatures caused by Joule heating in a closely-located electrical pulse source. The effect of temperature-dependent leakage current on threshold, efficiency, and hence output power has been analysed. The laser performance at elevated temperatures has been shown to be substantially affected by the waveguiding properties of the bulk active layer. The threshold current is shown to decrease, and the injection efficiency (limited by the current leakage), to increase, with the thickness of the active layer within a relatively broad range of both d_a and temperature increase. At small to moderate pumping levels, this means that highest power levels are achieved in laser structures with moderately thick active layers ($d_a\sim 0.06\ \mu\text{m}$). At higher injection levels, somewhat smaller d_a values may be advantageous, due to the less localised mode resulting in less stringent Catastrophic Optical Degradation limitations. Some of the tendencies considered (the importance of leakage and COD) are largely specific to the material system considered; others (the importance of the waveguiding properties of the active layer, leading to the substantially superlinear dependence $\Gamma_a(d_a)$, in defining the threshold current and efficiency at both room and elevated temperatures) are generic. Thus moderately thick (bulk) active layers located near the p -cladding can be expected to be beneficial for elevated-temperature operation of lasers with a similar structure realised in other material systems and operating at different wavelengths.

Authors' contributions Both authors contributed to analytical and numerical calculations as well as writing the paper

Funding None

Availability of data and materials Available on request

Declarations

Conflict of interests None

Ethical Approval Not applicable

Open Access This article is licensed under a Creative Commons Attribution 4.0 International License, which permits use, sharing, adaptation, distribution and reproduction in any medium or format, as long as you give appropriate credit to the original author(s) and the source, provide a link to the Creative Commons licence, and indicate if changes were made. The images or other third party material in this article are included in the article's Creative Commons licence, unless indicated otherwise in a credit line to the material. If material is not included in the article's Creative Commons licence and your intended use is not permitted by statutory regulation or exceeds the permitted use, you will need to obtain permission directly from the copyright holder. To view a copy of this licence, visit <http://creativecommons.org/licenses/by/4.0/>.

References

- Agrawal, G.P., Dutta, N.K.: Semiconductor lasers, 2nd edn. VNH, New York (1993)
- Algorri, J.F., Ochoa, M., Roldán-Varona, P., Rodríguez-Cobo, L., López-Higuera, J.M.: Light technology for efficient and effective photodynamic therapy: a critical review. *Cancers* **13**, 3484 (2021)
- Avrutin, E.A., Ryvkin, B.S.: Semiconductor laser design with an asymmetric large optical cavity waveguide and a bulk active layer near p-cladding for efficient high-power red light emission. *Semicond. Sci. Technol.* **37**(12), 125002 (2022)
- Avrutin, E.A., Ryvkin, B.S., Kostamovaara, J.T.: AlGaAs/GaAs asymmetric-waveguide, short cavity laser diode design with a bulk active layer near the p-cladding for high pulsed power emission. *IET Optoelectron.* **15**(4), 194–199 (2021)
- Bour, D.: AlGaInP Quantum Well lasers. In: Zory, P.S. (ed.) *Quantum Well lasers*. Academic Press, San Diego, CA (1993)
- Bour, D.P., Treat, D.W., Thornton, R.L., Geels, R.S., Welch, D.F.: Drift leakage current in AlGaInP quantum-well lasers. *IEEE J. Quantum Electron.* **29**(5), 1337–1343 (1993)
- BouSanayeh, M., Jaeger, A., Schmid, W., Tautz, S., Brick, P., Streubel, K., Bacher, G.: Investigation of dark line defects induced by catastrophic optical damage in broad-area AlGaInP laser diodes. *Appl. Phys. Lett.* **89**, 101111 (2006). <https://doi.org/10.1063/1.2345225>
- Crump, P., Erbert, G., Wenzel, H., Frevert, C., Schultz, C.M., Hasler, K.H., Staske, R., Sumpf, B., Maasdorf, A., Bugge, F., Knigge, S., Trankle, G.: Efficient high-power laser diodes. *IEEE J. Sel. Top. Quantum Electron.* **19**, 1501211 (2013)
- Dumitrescu, M., Toivonen, M., Savolainen, P., Orsila, S., Pessa, M.: High-power edge emitting red laser diode optimisation using optical simulation. *Opt. Quantum Electron.* **31**, 1009–1030 (1999)
- Hagimoto, M., Miyamoto, S., Watanabe, K., Kimura, Y., Fukai, H., Kawanaka, S.: Single-mode 200mW 660nm to 690nm red laser diode for sensing and medical application. *Proc. SPIE* **11301**, 1130105 (2020). <https://doi.org/10.1117/12.2543953>
- Hagimoto, M., Miyamoto, S., Watanabe, K., Hashizume, M., Yano, K.: Red laser diodes explore the future of biomedical and quantum technology. *Proc. SPIE* **12440**, 124400 (2023)
- Hallman, L.W., Ryvkin, B.S., Avrutin, E.A., Aho, A.T.: High Power 15 μm Pulsed Laser Diode With Asymmetric Waveguide and Active Layer Near p-cladding. *IEEE Photon. Technol. Lett.* **31**(20), 1635–1638 (2019)
- Hallman, L.W., Ryvkin, B.S., Avrutin, E.A., Kostamovaara, J.T.: >25 W pulses from 1.5 μm double-asymmetric waveguide, 100 μm stripe laser diode with bulk active layer. *Electron. Lett.* **57**(23), 891–893 (2021). <https://doi.org/10.1049/el12.12298>
- Hasler, K.H., Wenzel, H., Crump, P., Knigge, S., Maasdorf, A., Platz, R., Staske, R., Erbert, G.: Comparative theoretical and experimental studies of two designs of high-power diode lasers. *Semicond. Sci. Technol.* **29**(4), 045010 (2014)
- Ishikawa, M., Shiozawa, H., Itaya, K., Hatakoshi, G., Uematsu, Y.: Temperature dependence of the threshold for InGaAlP visible laser diodes. *IEEE J. Quantum Electron.* **27**(1), 23–29 (1991)
- Kaul, T., Erbert, G., Klehr, A., Maasdorf, A., Martin, D., Crump, P.: Impact of carrier nonpinning effect on thermal power saturation in GaAs-based high power diode lasers. *IEEE J. Select. Top. Quantum Electron.* **25**(6), 1501910 (2019)
- Lichtenstein, N., Winterhoff, R., Scholz, F., Schweizer, H., Weiss, S., Hutter, M., Reichl, H.: The Impact of LOC Structures on 670-nm (Al)GaInP High-Power Lasers. *IEEE J. Select. Top. Quantum Electron.* **6**, 564–570 (2000)
- Miyamoto, Y., Umebayashi, Y., Nishisaka, T.: Comparison of phototoxicity mechanism between pulsed and continuous wave irradiation in photodynamic therapy. *J. Photochem. Photobiol. B: Biology* **53**(1), 53–59 (1999)
- Olshansky, R., Su, C.B., Manning, J., Powazinik, R.: Measurement of radiative and nonradiative recombination rates in InGaAsP and AlGaAs light sources. *IEEE J. Quantum Electron.* **20**(8), 838–854 (1984)
- Ryvkin, B.S., Avrutin, E.A., Kostamovaara, J.T.: Asymmetric-waveguide, short cavity designs with a bulk active layer for high pulsed power eye-safe spectral range laser diodes. *Semicond. Sci. Technol.* **35**(8), 085008 (2020)
- Sanchez, M., Gallego, D., Lamela, H.: Overdrive short pulse high peak power diode lasers without catastrophic optical damage. *IEEE Photon. J.* **13**(4), 1500507 (2021)
- Smowton, P.M., Thomson, J.D., Yin, M., Dewar, S.V., Blood, P., Bryce, A.C., Marsh, J.H., Hamilton, C.J., Button, C.C.: The effect of cladding layer thickness on large optical cavity 650-nm lasers. *IEEE J. Quantum Electron.* **38**(3), 295–290 (2002)
- Yamagata, Y., Yamada, Y., Muto, M., Sato, S., Nogawa, R., Sakamoto, A., Yamaguchi, M.: "915nm high power broad area laser diodes with ultra-small optical confinement based on asymmetric decoupled

confinement heterostructure (ADCH). In: Proc, p. 93480F. San Francisco, CA, USA, SPIE LASE (2015)

Publisher's Note Springer Nature remains neutral with regard to jurisdictional claims in published maps and institutional affiliations.